Materials Science & Engineering A 660 (2016) 139–147

Contents lists available at ScienceDirect

Materials Science & Engineering A

journal homepage: www.elsevier.com/locate/msea

Spall damage of a mild carbon steel: Effects of peak stress, strain rate and pulse duration

C. Li [a,b,c], B. Li [c,d], J.Y. Huang [c,d], H.H. Ma [d], M.H. Zhu [b], J. Zhu [a,*], S.N. Luo [c,b,**]

[a] College of Physical Science and Technology, Sichuan University, Chengdu, Sichuan 610064, PR China
[b] Key Laboratory of Advanced Technologies of Materials, Ministry of Education, Southwest Jiaotong University, Chengdu, Sichuan 610031, PR China
[c] The Peac Institute of Multiscale Sciences, Chengdu, Sichuan 610031, PR China
[d] CAS Key Laboratory of Mechanical Behavior and Design of Materials, Department of Modern Mechanics, University of Science and Technology of China, Hefei, Anhui 230027, PR China

ARTICLE INFO

Article history:
Received 10 September 2015
Received in revised form
25 February 2016
Accepted 26 February 2016
Available online 27 February 2016

Keywords:
Peak stress
Pulse duration
Strain rate
Mild carbon steel
Spallation
Microstructure

ABSTRACT

We investigate spall damage of a mild carbon steel under high strain-rate loading, regarding the effects of peak stress, strain rate, and pulse duration on spall strength and damage, as well as related microstructure features, using gas gun plate impact, laser velocimetry, and electron backscatter diffraction analysis. Our experiments demonstrate strong dependences of spall strength on peak stress and strain rate, and its weak dependence on pulse duration. We establish numerical relations between damage and peak stress or pulse duration. Brittle and ductile spall fracture modes are observed at different loading conditions. Damage nucleates at grain boundaries and triple junctions, either as transgranular cleavage cracks or voids.

1. Introduction

How materials respond to dynamic extremes including high stresses and high strain rates resulting from the propagation of shock waves via impact, is of paramount importance for understanding dynamic events such as ballistic impact, blast loading, aerospace debris impact, automobile crash, and geological events. Metallic materials subject to shock loading predominantly fail from spall when the dynamic tensile stress exceeds the strength of materials [1,2]. Such transient tensile loading is a result of interactions of release waves from impact, and causes nucleation, growth, coalescence of voids or cracks, and failure [3–6].

Spall strength (σ_{sp}) is normally estimated from free-surface velocity histories during plate impact. However, σ_{sp} is not an intrinsic material property, since it depends on loading conditions and sample geometry, in addition to microstructure [4,7]. An extensive array of experiments [7–12] have investigated spall strength under varying stress amplitudes, tensile strain rates and pulse durations, but obtained different and sometimes conflicting results. For example, Stevens and Tuler [10] studied the effect of shock compression on incipient spall strength of 1020 steel and 6061-T6 aluminum alloy using gas gun and exploding foil techniques, and showed that σ_{sp} is weakly dependent on magnitude of shock precompression, or peak stress (σ_H). Johnson et al. [11] examined spall fracture of copper for different pulse durations (τ) and tensile strain rates ($\dot{\varepsilon}$); their experiments and numerical simulations revealed little dependence of σ_{sp} on either τ or $\dot{\varepsilon}$. However, contradictory results were reported by Chen et al. [7] on spallation of aluminum with different microstructures over σ_H = 4–22 GPa: σ_{sp} varies with increasing σ_H and $\dot{\varepsilon}$, but does not depend on τ.

While spall strength and the extent of damage may depend on σ_H, $\dot{\varepsilon}$ and τ, their effects are often intertwined. It is highly desirable to investigate their individual effects, but controlling a shock wave with a single variable is nontrivial [7]. Consequently such experiments are rare. Microstructure also plays a key role in spall damage, and it is always beneficial to make connections between velocimetry measurements and microstructures in a single set of experiments [13–17]. In this work, we choose an important engineering material, a mild steel, to explore the individual effects of σ_H, $\dot{\varepsilon}$ and τ on spall strength and damage, as well as related microstructure features, via gas gun plate impact, laser velocimetry,

* Corresponding author.
** Corresponding author at: The Peac Institute of Multiscale Sciences, Chengdu, Sichuan 610031, PR China.
E-mail addresses: zhujun01@163.com (J. Zhu), sluo@pims.ac.cn, sluo@swjtu.cn (S.N. Luo).

http://dx.doi.org/10.1016/j.msea.2016.02.080
0921-5093/

and electron backscatter diffraction (EBSD) analysis [18]. Medium and low strain rate experiments with split Hopkinson tension bar (SHTB) and materials testing system (MTS) loading are also included as a complement. Our experiments demonstrate strong dependences of spall strength on peak stress and strain rate, and its weak dependence on pulse duration, establish numerical relations between damage and peak stress or pulse duration, and reveal brittle and ductile spall fracture modes at different loading conditions.

2. Materials and experiments

The material used in this work is a mild carbon steel (Chinese steel Q235) similar to AISI 1020 mild steel [19], which contains 0.17% C, 1.3% Mn, 0.30% Si, 0.04% S, 0.04% P, and 97.8–98.1% Fe, by weight percentage. The grains are equiaxial with a mean grain size of ~30 μm (Fig. 1a). At room temperature and pressure, it has a density $\rho_0 = 7.85\ \mathrm{g\,cm^{-3}}$, longitudinal sound velocity $C_L = 5.95\ \mathrm{km\,s^{-1}}$, bulk sound velocity $C_B = 4.58\ \mathrm{km\,s^{-1}}$ [12], and Poisson's ratio $\nu = 0.3$.

Flyer plate impact experiments [20,21] are conducted with single-stage gas guns. The schematic setup of the impact experiments is shown in Fig. 1b. A flyer plate (3) is attached to a polycarbonate sabot (1), with a recess (2) immediately behind it. When a solenoid valve is fired, compressed gas (N_2 or He) is released from a high-pressure gas reservoir into the gun barrel (9), accelerating the sabot and flyer plate assembly. Upon exiting the muzzle, the flyer plate impacts the target or sample under consideration (4). The flyer plate velocity is measured with an optical beam blocking system (8), and the free surface velocity u_{fs} of the target, with a Doppler pin system or DPS (7). DPS is essentially a displacement interferometer similar to a photon Doppler velocimeter. The muzzle, target, and DPS probes including related optics are located in a vacuum chamber (10). The shock-loaded target is "soft-recovered" for post-mortem examinations [15,22–25]. Our "soft catch" system (12) is a 10 cm-deep-cylinder filled with soft vacuum sealant. Upon impact, the sabot is blocked, while the target flies into the cylinder and soft-caught by the sealant. Most of the samples are recovered "intact" except thin ones. The additional microstructure changes during the soft-catch are expected to be small. The tilt of impact is 5–10 mrad as determined from multipoint DPS measurements.

Two parallel surfaces of a flyer plate/target disk are polished to micron level or mirror finish. Both flyer plates and targets are made of the mild steel for symmetric impact. The diameters of the flyer plates and targets are 10–14 mm. The impact experiments are divided into three groups, i.e., the pulse duration, strain rate and peak stress groups (Table 1). The pulse duration group examines pulse duration effect on spall strength, and the flyer plate thickness is varied while the sample thickness and flyer plate or impact velocity (u_f) are fixed. A nominal duration, normally defined as t_{CD} in Fig. 2a, is used to quantify the loading pulse duration. The strain rate group is intended to investigate strain rate effect. While the flyer plate/target thickness ratio is fixed at 1:2 and u_f remains at ~400 m s^{-1}, we vary the thicknesses of the flyer plate and target to achieve different strain rates. To explore peak stress effect (the peak stress group), we fix the nominal thicknesses of flyer plates and targets at 1 mm and 2 mm, respectively, and vary the flyer plate velocity. The uncertainties in flyer plate and free surface velocity measurements are within 1%.

In order to compare with high strain rate gas gun experiments, we also perform tension experiments at low strain rates (10^{-3}–$10^{-2}\ \mathrm{s^{-1}}$) with a materials' testing system, and at medium strain rates ($10^{3}\ \mathrm{s^{-1}}$) with a split Hopkinson tension bar. The samples are of a dog-bone shape, and their gauge dimensions are 5 mm × 2 mm. The tensile strengths at low and medium strain rates are obtained from the true stress–strain curves. Details of such experiments and data processing are presented elsewhere [26].

The samples are recovered from gas gun, MTS and SHTB experiments for scanning electron microscopy (SEM) and EBSD characterizations. Samples recovered from gas gun experiments are sectioned into two halves along the shock loading direction, ground and polished with 1 and 0.3 μm alumina particles, and then electro-polished in 5% perchloric acid and 95% ethanol at 50 V, with a Cu rod and the sample as electrodes. EBSD characterization is performed in a FEI Quanta 250 FEG-SEM equipped with Oxford EBSD detector and HKL channel 5 OIM software, with a 30 kV voltage, 15 mm working distance, and 70° tilt. Regions of interest for SEM and EBSD are in the central portion not affected by edge release.

3. Results and discussion

Representative free surface velocity profiles, $u_{fs}(t)$, for three groups of experiments, i.e., the pulse duration, strain rate, and peak stress groups, are presented in Fig. 2a–c, respectively. Here t

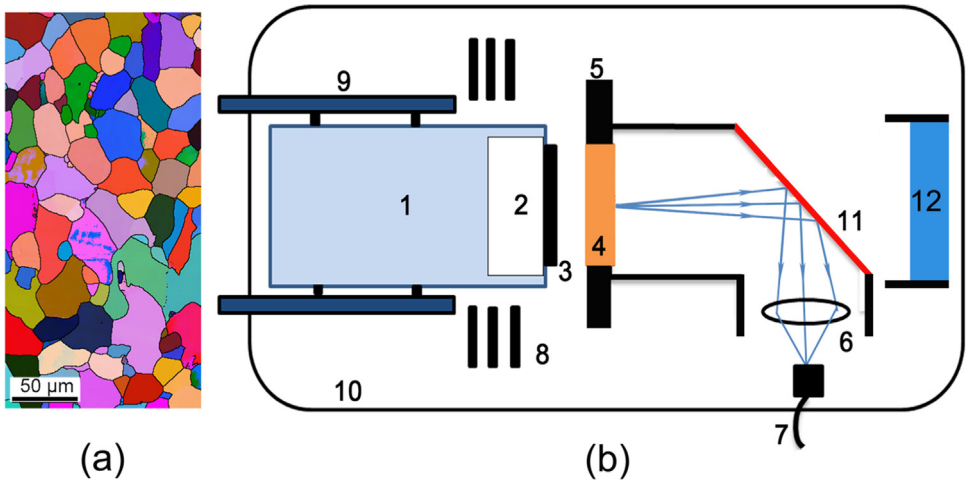

Fig. 1. (a) EBSD orientation map of an as-received carbon steel specimen. (b) Schematic setup of gas gun flyer-plate impact experiments. 1: polycarbonate sabot; 2: recess for release waves; 3: flyer plate; 4: sample; 5: sample holder; 6: lens; 7: optical fiber connected to the Doppler pin system (DPS) probe; 8: optical fibers and detectors for the optical beam block system; 9: gun barrel; 10: vacuum/target chamber; 11: thin mirror; 12: soft recovery.